Am J Nucl Med Mol Imaging 2025;15(1):28-36
www.ajnmmi.us /ISSN:2160-8407/ajnmmi0156717

Original Article

Metabolic parameters analysis of ^{18}F-FDG PET/CT in the diagnosis and differential diagnosis of collecting duct carcinoma

Yongkang Qiu[1*], Xiaoyue Zhang[1*], Jia Cheng[1], Wenpeng Huang[1], Zhao Chen[1], Lele Song[1], Qi Yang[1], Xinyao Sun[1], Aixiang Wang[2], Tianyao Wang[1], Lei Kang[1]

[1]Department of Nuclear Medicine, Peking University First Hospital, Beijing 100034, China; [2]Department of Urology Pathology, Peking University First Hospital, Beijing 100034, China. [*]Equal contributors.

Received March 21, 2024; Accepted January 6, 2025; Epub February 25, 2025; Published February 28, 2025

Abstract: Purpose: This study aims to explore the diagnostic performance of ^{18}F-FDG PET/CT in distinguishing collecting duct carcinoma (CDC) from clear cell renal cell carcinoma (ccRCC). Methods: A retrospective analysis was conducted on 11 patients with CDC and 27 patients with ccRCC who underwent ^{18}F-FDG PET/CT examinations. Clinical indicators and the SUVmax, tumor-to-liver standardized uptake value ratio (TLR), tumor-to-kidney standardized uptake value ratio (TKR), metabolic tumor volume (MTV) and total lesion glycolysis (TLG) values of the primary tumor, whole-body MTV (WBMTV), and whole-body TLG (WBTLG) based on a baseline PET scan, were recorded and compared between the two groups. To assess the discriminative power of these metabolic parameters between CDC and ccRCC, we performed a receiver operating characteristic (ROC) curve analysis. Results: The median age of the 11 CDC patients was 59 years. All CDC patients were in advanced stages (18% stage III and 82% stage IV). Compare with ccRCC patients, CDC patients had higher lymph node metastases rates (72.7% vs. 22.2%, $P = 0.008$) and distant metastases rates (81.8% vs. 22.2%, $P = 0.001$). The primary tumor in CDC also showed higher SUVmax (10.5 vs. 4.0, $P < 0.001$), TLR (3.9 vs. 1.4, $P < 0.001$), TKR (4.4 vs. 1.5, $P < 0.001$), MTV (53.2 vs. 9.5, $P = 0.021$), and TLG (305.7 vs. 30.4, $P = 0.0069$) than ccRCC. The WBMTV and WBTLG of CDC patients were also higher than the ccRCC group (144.1 vs. 9.5, $P = 0.0013$ and 528.4 vs. 30.4, $P = 0.0013$, respectively). ROC curve analysis revealed no significant differences in the ability of SUVmax, TLR and TKR to differentiate CDC from ccRCC. Median survival for CDC was 36 months, worse for older patients. Conclusion: The utilization of ^{18}F-FDG PET/CT can assist to detect the metastases and provide guidance for diagnosis and staging. Metabolic parameters obtained from ^{18}F-FDG PET/CT hold promise for distinguishing CDC from ccRCC.

Keywords: Collecting duct carcinoma, ^{18}F-FDG, PET/CT, tumor-to-liver standardized uptake value ratio (TLR), tumor-to-kidney standardized uptake value ratio (TKR)

Introduction

Collecting duct carcinoma (CDC) stands as a rare kidney tumor variant, constituting less than 2% of diagnosed cases within the clinical landscape [1, 2]. It predominantly affects men with the male-to-female ratio of 2:1 [3]. The age of presentation varies between 14 and 89 years with a median age of 59 years [4]. CDC is known for its aggressive nature, often presenting as a high-grade, advanced-stage tumor with lymph node involvement and distant metastases, which are often found in the lungs, bones, liver, and other organs [3, 5]. In general, the prognosis for CDC is poor, typified by a median survival duration ranging from 13.2 to 16 months [3, 4].

The standard treatment approach for this type of cancer involves cytoreductive nephrectomy, with or without adjuvant chemotherapy and radiation [4]. However, early distant metastases were often detected in patients with CDC, making surgical intervention alone unlikely to achieve a complete cure for the majority of patients. According to current evidence, the traditional therapies commonly used for RCC, such as sunitinib and sorafenib, have shown limited effectiveness against this particular cancer subtype [6, 7]. The available chemotherapy options for this disease also demonstrated limited efficacy, underscoring the critical importance of early detection as the most impactful strategy for prolonging patient survival [1, 8].

Ultrasonography has been utilized to identify the solid and cystic components of renal masses [9]. However, due to the infiltrative growth pattern of CDC, it can sometimes lead to missed diagnoses as the early stage may preserve the intact renal contour without obvious mass formation. For the detection and evaluation of renal tumors, especially smaller ones, computed tomography (CT) stands as a primary imaging technique [10, 11]. In contrast, magnetic resonance imaging (MRI) boasts excellent soft tissue resolution and does not pose any radiation-related risks. It allows for an earlier detection of internal necrosis within the lesions, differentiates pseudo-capsules at the lesion margins, and outperforms CT in its ability to distinguish between benign and malignant lesions, as well as demonstrating tumor thrombus and invasion of surrounding organs [9]. Nevertheless, both MRI and CT face challenges in detecting multiple systemic metastases of CDC. Given the low incidence of CDC, further

https://doi.org/10.62347/KQJB5668

research and summary of its radiological characteristics are needed to improve the precision of its radiological diagnosis.

^{18}F-Fluorodeoxyglucose (^{18}F-FDG) positron emission tomography (PET)/CT has gained significant utility in the realms of tumor identification, preoperative staging, postoperative reassessment, and treatment response monitoring. While most renal cell carcinomas exhibit subdued ^{18}F-FDG metabolism akin to normal renal tissue, with subsequent renal excretion of ^{18}F-FDG, CDC stands apart due to its pronounced invasiveness and heightened propensity for metastases at the point of initial diagnosis [12]. Nonetheless, there remains limited documentation of CDC features discernible through ^{18}F-FDG PET/CT. Recently, ^{18}F-FDG PET/CT volume-based parameters such as maximum standardized uptake value (SUVmax), metabolic tumor volume (MTV) and total lesion glycolysis (TLG) were used as prognostic factors for metastatic RCC [13]. However, there exists a limited body of research examining volume-based parameters in CDC patients. This study endeavors to explore the diagnostic capabilities of ^{18}F-FDG PET/CT and its value in distinguishing CDC from clear cell renal cell carcinoma (ccRCC).

Material and methods

Patients

We retrospectively reviewed the medical records of 11 CDC patients who underwent ^{18}F-FDG PET/CT in Peking University First Hospital between October 2015 and July 2023. The study enrollment criteria included several key elements: firstly, the requirement for a definitive pathological diagnosis confirming the primary tumor as either CDC or ccRCC; secondly, the mandate that the nephrectomy or core needle biopsy procedures be conducted within our hospital; thirdly, the essential condition of ^{18}F-FDG PET/CT administration prior to nephrectomy or initiation of systemic treatment; and lastly, the stipulation of a time interval of no more than five weeks between the ^{18}F-FDG PET/CT scan and the histopathological diagnosis. Furthermore, we extended our investigation to include the retrospective review of medical records pertaining to 27 ccRCC patients who underwent ^{18}F-FDG PET/CT examinations within the timeframe spanning November 2020 to May 2022 in our hospital. The same inclusion criteria, as applied to the cohort of CDC patients, were employed in the assessment of this additional patient subset.

Clinical indicators such as age, gender, and blood glucose were recorded. Follow-up data is gathered through either outpatient follow-up reviews or telephone follow-up interviews. Before analysis, the medical records of the enrolled patients were subjected to a process of anonymization and de-identification to safeguard their privacy. This retrospective investigation received approval from our hospital's ethics committee, and it was determined that written informed consent was not required.

^{18}F-FDG PET/CT examination

Prior to the examination, all patients were subjected to a minimum 6-hour fasting period. The ^{18}F-FDG PET/CT scan was conducted using a uMI 780 PET/CT scanner (United Imaging Healthcare, Shanghai). The administration of ^{18}F-FDG (3.7 MBq/kg body weight, provided by Atom high-tech Co., Ltd., Beijing, China) intravenously preceded the scan by 60-80 minutes. During the examination, images were acquired in the supine position. The process involved both plain CT and PET scans. The CT scan, devoid of contrast medium, was conducted at 130 keV, 80 mAs, and featured a slice thickness of 3.0 mm. Subsequently, a PET scan was conducted with a matrix size of 200 × 200, incorporating corrections for dead time, scatter, and decay. This PET scan necessitated eight bed positions, each lasting 3 minutes. The collected images underwent an iterative reconstruction process using the OSEM algorithm. Additionally, Gaussian filtering was applied to achieve an in-plane spatial resolution of 5 mm at full-width and half-maximum, while CT-based attenuation correction was also incorporated.

PET/CT images analysis

Two proficient nuclear medicine practitioners, without prior knowledge of any clinical details pertaining to the patients, independently evaluated the PET/CT images. In case of discordant outcomes, they engaged in comprehensive discussions to deliberate upon the observations, ultimately arriving at a mutually agreed-upon conclusion. The region of interest (ROI) chosen for analysis was determined based on the presence of abnormal radiotracer accumulation as observed on the PET/CT images. To ensure accuracy, the slice exhibiting the highest uptake of ^{18}F-FDG was selected, taking care to exclude any physiological uptake. For the primary renal lesion and all metastatic lesions, the computer algorithm automatically calculated the SUVmax within the defined ROI. Additionally, MTV and TLG were also acquired with a SUV threshold as 2.5. Subsequently, we calculated the MTV and TLG values from the local kidney lesion and all metastatic lesions to derive the parameters for whole-body MTV (WBMTV) and whole-body TLG (WBTLG).

A circular ROI measuring 1 cm in diameter was drawn within the right lobe of the liver and in the corresponding healthy renal tissue, deliberately placed at a distance from the primary lesion to ensure accuracy. Subsequently, the tumor-to-liver ratio (TLR), as well as the tumor-to-kidney ratio (TKR), were computed. The primary lesion's tumor size was determined by measuring its maximum dimension. The assessment of regional lymph nodes and the presence of distant metastases followed the guide-

Table 1. Patients and lesions characteristics

Patient	Age	Tumor side	Size (mm)	SUVmax	TLR	TKR	MTV	TLG	WBMTV	WBTLG	Regional lymph node metastases	Distant metastasis location	pStage	Follow-up	
														Status	Time (mo)
1	66	L	84	25.1	8.10	7.17	91.21	662.36	98.226	427.659	+	Lung, bone (5th left rib)	IV	A	6
2	27	R	107	31.8	20.40	12.97	495.83	5647.84	790.38	4956.62	-	Bone (multiple)	IV	L	1
3	67	L	87	4.1	1.52	1.05	18.24	63.1	51.65	123.01	+	Lung, bone (6th left rib), distant lymph node	IV	D	10
4	50	R	61	5.5	1.80	2.14	116.2	404.9	118.95	434.49	+	-	III	D	47
5	53	R	76	20.5	11.60	8.23	269.25	2449.15	569.21	3415.35	+	Lung, bone (multiple)	IV	D	36
6	66	R	72	14.4	6.54	5.76	53.18	305.67	61.66	516.79	+	-	III	D	8
7	80	L	59	7.0	2.22	2.67	39.23	137.52	273.67	812.91	-	Lung, bone (multiple)	IV	D	9
8	59	L	24	5.7	2.13	2.21	1.73	5.85	11.93	43.32	+	Distant lymph node	IV	A	12
9	52	R	89	29.0	13.81	10.00	190.91	2170.53	191.74	1528.08	-	Serratus anterior muscle	IV	A	33
10	63	L	48	8.9	3.78	4.14	9.92	42.71	144.07	528.37	+	Lung, liver, distant lymph node	IV	D	1
11	37	R	51	10.5	3.89	4.43	52.79	233.72	243.74	1333.38	+	Lung, pleura, peritoneum, bone (multiple), distant lymph node, muscle	IV	A	1

A = Alive; L = Loss to Follow-up; D = Death.

Table 2. Comparison of clinical characteristics between CDC and ccRCC

Characteristic	CDC (N = 11)	ccRCC (N = 27)	*P* Value
Clinical parameters			
Age (years)	59 (50.0-66.0)	64.0 (51.0-72.0)	0.247[a]
Blood glucose (mmol/L)	5.6 (5.0-6.9)	5.6 (5.2-6.2)	0.401[a]
Primary tumor size (mm)	72 (51-87)	65 (49-77)	0.485[b]
Gender			0.073[c]
Male	7 (63.6%)	8 (29.6%)	
Female	4 (36.4%)	19 (70.4%)	
Regional lymph node metastases	8 (72.7%)	6 (22.2%)	*0.008*[c]
Distant metastases	9 (81.8%)	6 (22.2%)	*0.001*[c]

Continuous variables are presented as median (interquartile range), while categorical variables are expressed as percentages. *P* value < 0.05 was highlighted in italics. [a]Student t-test. [b]Mann-Whitney U-test. [c]Fisher exact test.

lines outlined in the eighth edition of the American Joint Committee on Cancer (AJCC) TNM staging system.

Statistical analysis

To assess the continuous variables in both the CDC and ccRCC groups, either the Mann-Whitney U-test or the Student's test was utilized according to normality test. The Fisher exact test was employed for the comparison of independent categorical variables. To determine the optimal cutoff value and area under the curve (AUC) for each continuous variable, receiver operating characteristic (ROC) curve analysis was employed, with the AUC tested using the DeLong method. Kaplan-Meier analysis was performed using Kaplan-Meier Plotter. Survival rates were determined according to overall survival. The statistical analyses were carried out using Rstudio (Version 2023.03.1.446, RStudio, Inc., Boston, MA, USA) or SPSS Statistics software (version 25.0; SPSS, corporation, Chicago, IL, USA). A significance level of $P < 0.05$ was used to determine statistical significance.

Results

General characteristics

Eleven patients with newly diagnosed CDC were enrolled. The pertinent attributes of both patients and their associated lesions have been outlined in **Table 1**. The median age of diagnosis was 59 years, with an age range spanning from 27 to 80 years. A predominant proportion of the patients were male, constituting 63.6% (7/11). Notably, all patients were diagnosed with the disease at an advanced stage, with 18% classified as stage III and 82% as stage IV. Moreover, an additional group of twenty-seven patients with newly diagnosed ccRCC were also included in the study. This subgroup included 8 males (29.6%) and 19 females (70.4%), with the median age at diagnosis of 63 years (range: 32-80). The comparative analysis outlined in **Table 2** reveals no statistically significant differences in age distribution, gender ratio, and blood glucose levels between the two groups ($P > 0.05$).

Comparison of clinical characteristics between CDC and ccRCC

The median sizes of the primary tumors for CDC and ccRCC were 72 mm (range: 24-107 mm) and 65 mm (range: 23-130 mm), respectively. Notably, no statistically significant disparity was discerned between these two cohorts ($P > 0.05$). In terms of lymph node metastases, 72.7% (8/11) of patients with CDC exhibited regional lymph node metastases, whereas only 22.2% (6/27) of patients with ccRCC displayed regional lymph node metastases (**Table 2**). Distant metastases were noted in 81.8% (9/11) CDC patients, with the lung (54.5%, 6/11) and bone (54.5%, 6/11) being the most common sites of distant metastases. Other sites of distant metastases included remote lymph node (36.4%, 4/11), muscle (18.2%, 2/11), liver (9.1%, 1/11), pleura (9.1%, 1/11) and peritoneum (9.1%, 1/11) (**Table 1**). Among the ccRCC patients, distant metastases were only detected in 22.2% (6/27) cases. The two groups demonstrated statistically significant differences in terms of both lymph node metastases ($P = 0.008$) and distant metastases ($P = 0.001$) as indicated in **Table 2**. Representative cases of CDC and ccRCC are shown in **Figure 1**.

Comparison of metabolic parameters between CDC and ccRCC

CDC exhibited a notable increase in ^{18}F-FDG uptake, as evidenced by a median SUVmax of 10.5 (range: 4.1-31.8), a distinction that proved to be statistically significant when contrasted with ccRCC ($P < 0.001$) as depicted in **Figure 2A**. Notably, this distinction endured its statistical significance even after correction by liver ($P < 0.001$) or ipsilateral normal renal parenchyma ($P < 0.001$) background noise as shown in **Figure 2B** and **2C**. MTV (53.2 vs. 9.5, $P = 0.021$) (**Figure 2D**), and TLG (305.7 vs. 30.4, $P = 0.0069$) (**Figure 2E**) were found to be significantly elevated within the CDC group compared to the ccRCC group (**Table 3**). Moreover, WBMTV (144.1 vs. 9.5, $P = 0.0013$) (**Figure 2F**) and WBTLG (528.4 vs. 30.4, $P = 0.0013$) (**Figure 2G**) exhibited marked elevation in the CDC group as compared to their ccRCC counterparts (**Table 3**). In **Figure 3**, we present a comparative analysis of ^{18}F-FDG PET/CT images from patients with CDC and ccRCC, featuring similar primary tumor sizes.

ROC curve analyses were employed to assess the discriminative capacity of primary tumor SUVmax, TLR, and TKR in distinguishing between CDC and ccRCC (**Figure 4**).

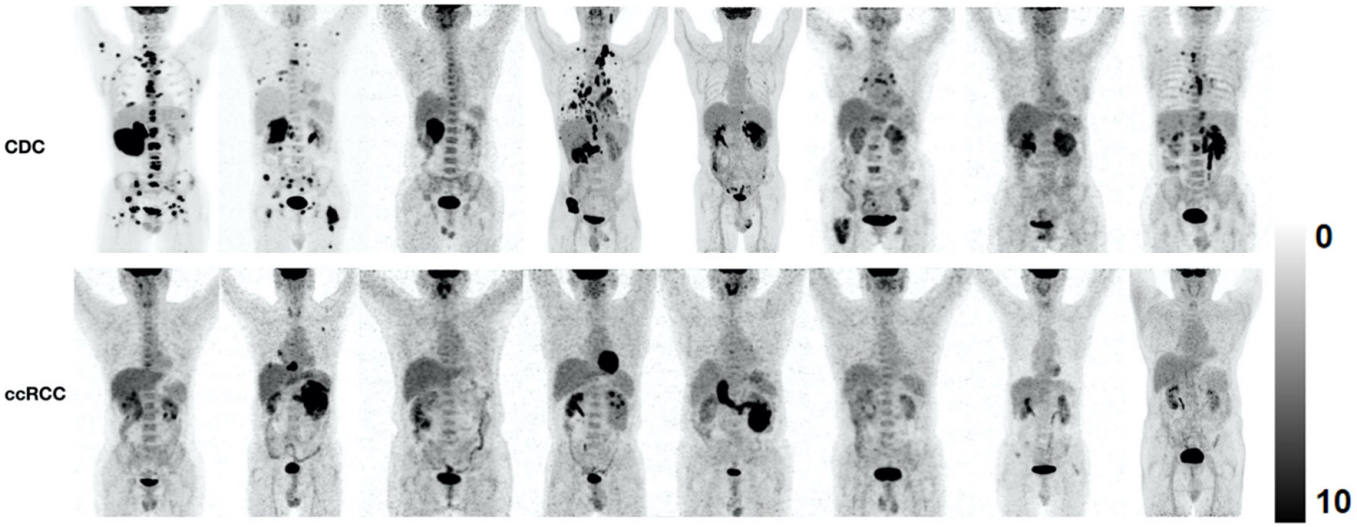

Figure 1. MIP images of representative CDC and ccRCC cases.

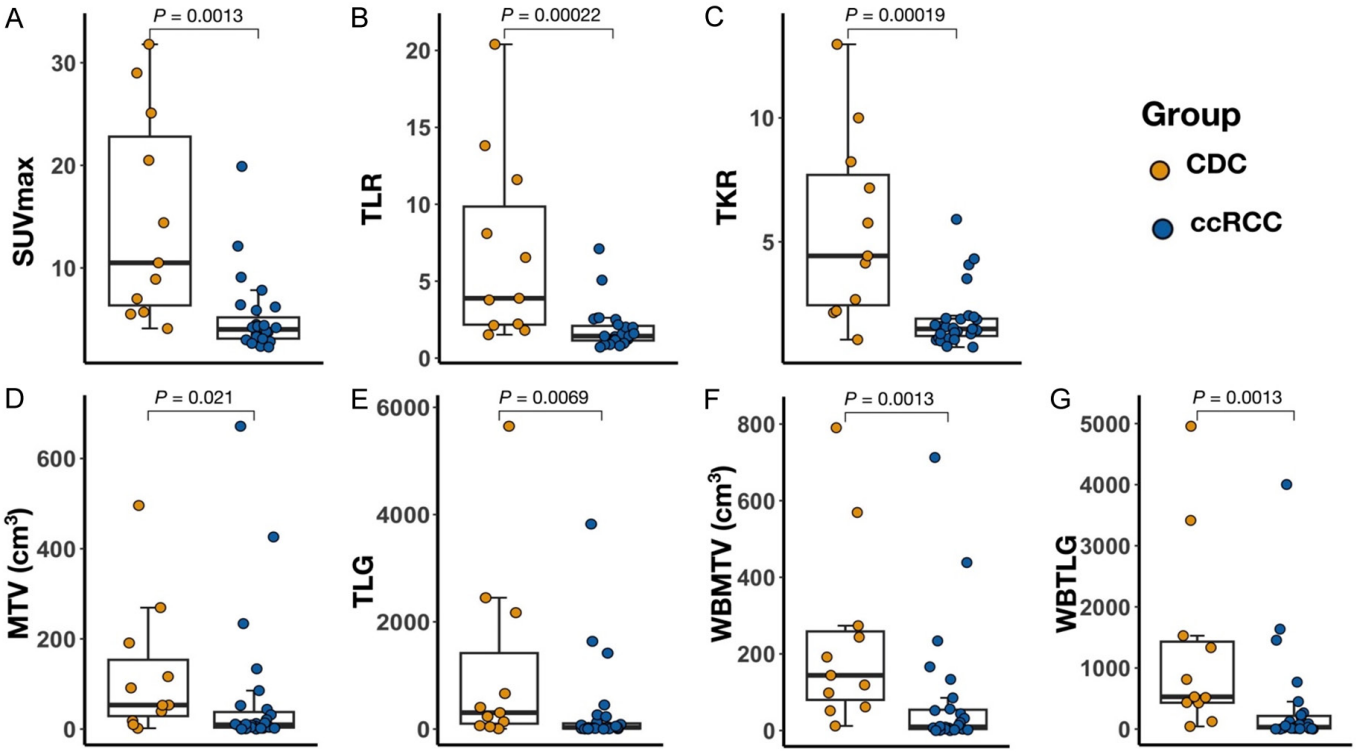

Figure 2. Comparisons of SUVmax (A), TLR (B), TKR (C), MTV (D), TLG (E), WBMTV (F) and WBTLG (G) between the CDC and ccRCC. Significant differences of SUVmax, TLR, TKR, MTV, TLG, WBMTV and WBTLG were observed between the CDC and ccRCC groups.

The results, including optimal cutoff values, AUCs, and associated *P* values, have been summarized in **Table 4**. According to the DeLong test, there was no statistically significant difference observed among the SUVmax (AUC: 0.875), TLR (AUC: 0.869), and TKR (AUC: 0.865) when it came to distinguishing between CDC and ccRCC.

Survival

The median follow-up time was 9.5 months, with a range spanning from 1 to 47 months. Overall, 6 deaths were observed among 10 patients diagnosed with CDC. All causes of death were progressive disease. The median overall survival stood at 36 months (95% CI, 8.26-63.74) (**Figure 5A**). Kaplan-Meier analysis demonstrated that the elder patients have poorer prognosis (Delong test *P* = 0.006) than those younger patients (**Figure 5B**).

Discussion

CDC, an uncommon renal cell carcinoma variant, is often associated with a poor prognosis and is frequently

Table 3. Comparison PET/CT parameters between CDC and ccRCC

Characteristic	CDC (N = 11)	ccRCC (N = 27)	*P* Value*
PET/CT parameters			
SUVmax	10.5 (5.7-25.1)	4.0 (3.1-5.9)	*< 0.001*
TLR	3.9 (2.1-11.6)	1.4 (1.1-2.2)	*< 0.001*
TKR	4.4 (2.2-8.2)	1.5 (1.1-1.9)	*< 0.001*
MTV	53.2 (18.2-190.9)	9.5 (2.9-43.8)	*0.021*
TLG	305.7 (63.1-2170.5)	30.4 (8.8-124.3)	*0.0069*
WBMTV	144.1 (61.7-273.7)	9.5 (3.8-56.1)	*0.0013*
WBTLG	528.4 (427.7-1528.1)	30.4 (10.3-231.0)	*0.0013*

SUVmax, maximum standardized uptake value; TLR, tumor-to-liver standardized uptake value ratio; TKR, tumor-to-kidney standardized uptake value ratio; MTV, metabolic tumor volume; TLG, total lesion glycolysis; WBMTV, whole-body MTV; WBTLG, whole-body TLG. Continuous variables are presented as median (interquartile range). *P* value < 0.05 was highlighted in italics. *Mann-Whitney U-test.

detected at an advanced stage marked by metastasis. The study encompassed a diverse patient population in terms of age, revealing a median age of 61 years at the point of diagnosis. Additionally, a modestly elevated male-to-female ratio of 3:2 was noted, aligning with previously documented research findings [14]. However, it is important to note that this demographic profile is not unique to the CDC, but rather reflects the overall characteristics of RCC. As a result, this particular demographic profile does not possess discriminatory significance in distinguishing the studied subtype from other subtypes.

Up to now, there is limited information regarding the PET/CT performance in CDC due to its rarity. To address this gap, compiled the preoperative PET/CT findings of ten patients with CDC and compared them with ccRCC patients. Firstly, CDC is mostly located in the renal medulla, with possible involvement of the renal cortex and renal pelvis [15]. The tumor lacks clear boundaries with the surrounding normal renal tissue [16, 17], consequently, it may lead to alterations in the contour of the affected kidney and invade the perirenal tissues, resulting in thickening of the perirenal fascia [18]. However, most of ccRCC exhibit expansive growth [8]. Due to compression of the surrounding kidney tissue by the tumor, ischemia and fibrous tissue proliferation occur, forming a pseudo-capsule [19]. Therefore, unlike CDC, ccRCC often appears with clear margins, with minimal involvement of the renal capsule, perirenal fat space, or renal fascia [17].

CDC generally exhibits a notable increase in ^{18}F-FDG uptake, as supported by multiple studies [12, 19, 20]. Ye et al. [21] reported a case with a CDC tumor showing high metabolic activity with an SUVmax of 7.0 [21]. Similarly, in a reasearch by Lyu et al. [19], two patients underwent PET/CT examination had highly metabolic primary lesions, as evidenced by SUVmax values of 14.9 and 14.3. Hu et al. [12] also reported two CDC patients with a noticeable increase in ^{18}F-FDG uptake within their tumors. The SUVmax of the primary lesions in all of our patients is greater than 5. According to a meta-analysis of 14 studies, only 62% of RCC lesions revealed increased FDG uptake [22]. Additionally, a significant portion of primary soft-tissue renal masses among all cases of RCC exhibited mild FDG uptake, which closely resembled the uptake seen in normal renal parenchyma [23, 24]. In summary, ^{18}F-FDG uptake was generally higher in CDC than in CCRCC. These research results are consistent with our observations.

CDC has a propensity for early local lymph node metastases and distant hematogenous metastases, indicating its aggressive nature [18]. Early detection of metastases is crucial for determining the treatment approach and improving patient outcomes [25]. PET/CT has demonstrated its effectiveness in identifying metastases in renal tumors, including CDC. Safaei et al. [26] reported a high sensitivity (87%) and specificity (100%) of PET in detecting metastases in RCC. Furthermore, Majhail et al. [27] found that ^{18}F-FDG PET/CT had a specificity and positive predictive value of 100% for distant metastases in patients with RCC. Li et al. [28] reported a case of CDC with abnormal ^{18}F-FDG uptake observed within subcutaneous soft tissue, muscles and bones. In a CDC case reported by Marx et al. [29], PET/CT imaging unveiled strong tracer absorption in numerous metastatic sites, including those found in the bone, lymph nodes, and lung. Similarly, high ^{18}F-FDG uptake in the multiple lymph node metastases was described in a case reported by Bertagna et al. [30] Our study revealed marked ^{18}F-FDG uptake in lymph nodes, lung, bone, liver, adrenal gland and muscle, indicating the capacity of ^{18}F-FDG PET/CT in identifying metastatic spread of CDC. The ability to detect metastases preoperatively can aid in decision-making regarding surgical intervention, leading to improved patient outcomes. Moreover, CDC would benefit from ^{18}F-FDG PET/CT in evaluating subsequent systemic therapy response.

In terms of contrast-enhanced CT characteristics, CDC typically showed slight enhancement and sometimes appeared as thickened enhancing internal septations and mural soft-tissue nodules. On magnetic resonance imaging (MRI), CDC always appeared hypointense on T1 and T2 weighted images [17, 19]. However, CT or MRI findings are nonspecific and do not distinguish collecting duct carcinoma from other subtypes of renal-cell carcinoma. ^{18}F-FDG PET/CT can detect high FDG uptake and early metastasis of CDC lesions, which shows advantages in diagnosis and accurate staging.

To our knowledge, our study compares, for the first time, metabolic parameter including SUVmax, TLR, TKR, MTV, TLG, WBMTV and WBTLG between CDC and ccRCC. We

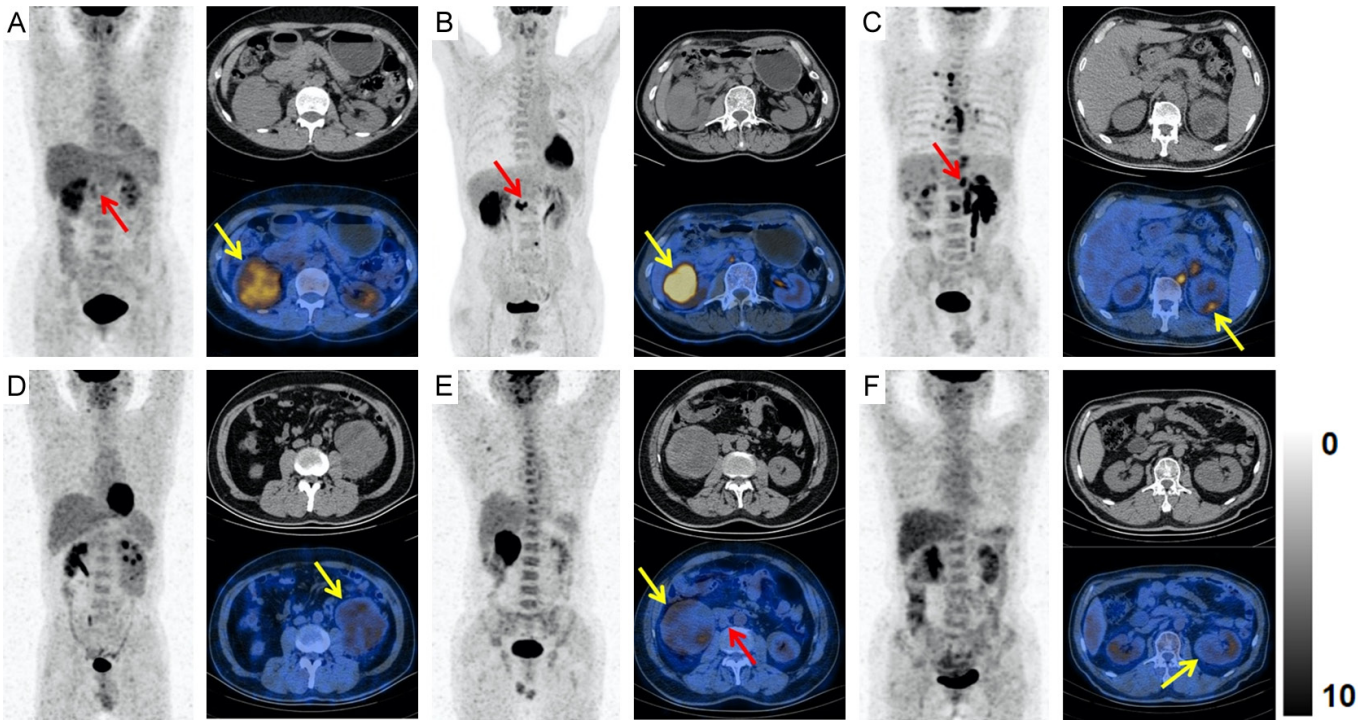

Figure 3. ^{18}F-FDG PET/CT images of the CDC and ccRCC patients with similar primary tumor size. The primary tumors were indicated by yellow arrows and the regional lymph node metastases were indicated by red arrows. A-C. Three CDC patients displayed primary tumor sizes of 61 mm, 72 mm, and 48 mm. The corresponding SUVmax values for these tumors were 5.5, 14.4, and 8.9, respectively. D-F. Three ccRCC patients showed primary tumor sizes of 89, 81 and 46 mm. The corresponding SUVmax values for these tumors were 4.2, 3.8, and 2.6, respectively.

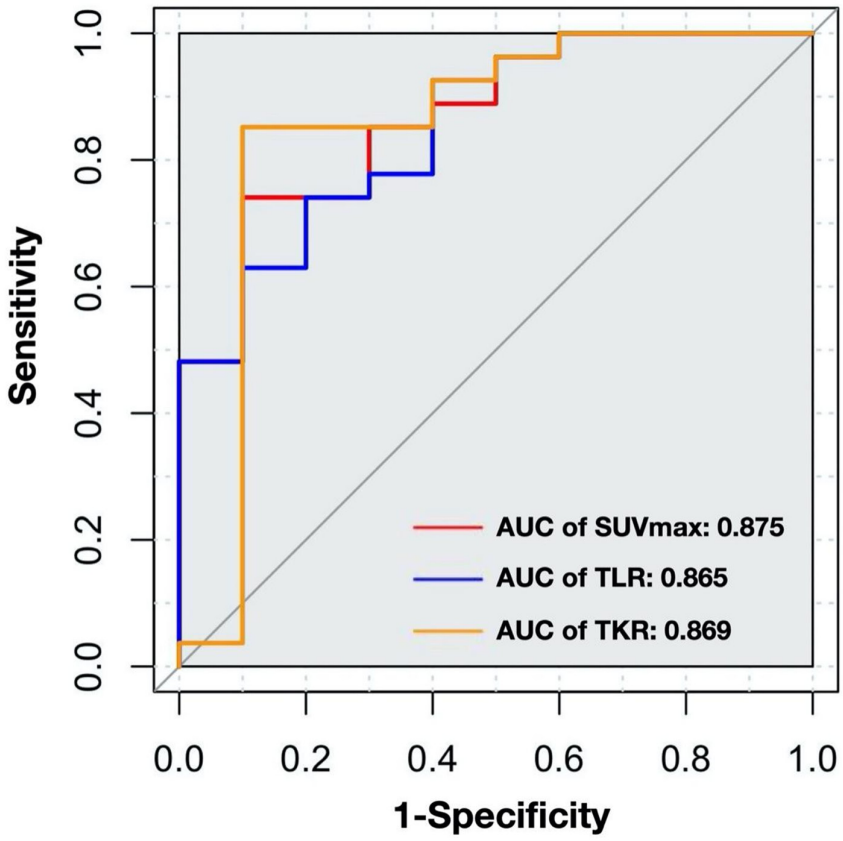

Figure 4. ROC curve analyses. SUVmax, TLR, TKR all demonstrated good discrimination ability between patients with the CDC and ccRCC.

found that SUVmax, TLR, and TKR can effectively differentiate between CDC and ccRCC. These findings indicate that ^{18}F-FDG PET/CT can provide valuable information on the metabolic activity and extent of CDC tumors, aiding in their detection, differential diagnosis, staging and therapeutic effect evaluation.

While our study provides valuable insights, there are limitations to consider. Firstly, the constrained sample size of ^{18}F-FDG PET/CT findings restricted our ability to conduct a comprehensive statistical analysis of the imaging observations, which may limit the generalizability of the results. Therefore, larger studies are necessary to establish more specific imaging criteria for CDC diagnosis. Additionally, the diagnosis of lymph node metastases and distant metastases is based on imaging findings, while challenges during surgery hinder the acquisition of pathological results for lymph nodes and distant organs, thereby preventing definitive confirmation of metastases.

Future studies should aim to overcome the limitations identified in our research.

Table 4. ROC curve analyses

Variables	Cutoff value	AUC	*P* value	95% CI	Sensitivity (%)	Specificity (%)
SUVmax	5.00	0.875	< 0.001	0.762-0.989	90.9	74.1
TLR	1.70	0.865	< 0.001	0.746-0.985	90.9	66.7
TKR	2.08	0.869	< 0.001	0.718-1.000	90.9	85.2

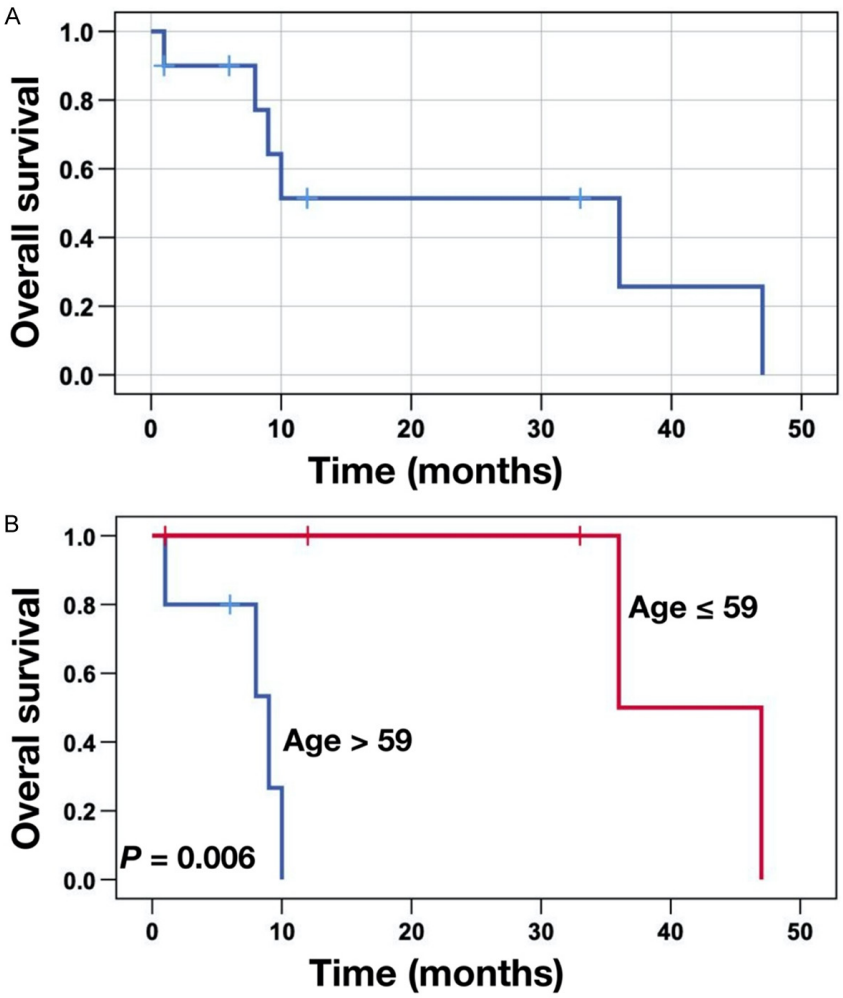

Figure 5. Overall survival of patients with CDC (A) and Kaplan-Meier analysis of age (B). Kaplan-Meier curve showed overall survival of all subjects (A). Time was expressed in months since the initial PET/CT scan. The cutoff value for age was defined as a median of 59. Elder patients had poorer prognosis (Delong test $P = 0.006$) than those younger patients (B).

Increasing the sample size and conducting comprehensive statistical analyses would enhance the reliability and generalizability of the findings. Moreover, specific imaging features unique to CDC need to be identified to differentiate it from other renal diseases. Additionally, it is imperative to conduct additional research to investigate the precision of ^{18}F-FDG PET/CT in identifying lymph node metastases and distant metastases. These advancements will improve the clinical utility of ^{18}F-FDG PET/CT, ultimately benefiting the management and prognostication of CDC patients. In addition, it is worth looking forward to further exploring the relationship between ^{18}F-FDG PET/CT features and prognosis of CDC through the analysis of large samples, and then predicting the prognosis of CDC patients by ^{18}F-FDG PET/CT at the time of diagnosis.

Conclusion

Our study highlights the potential of ^{18}F-FDG PET/CT metabolic parameters in distinguishing CDC from ccRCC. The preoperative use of ^{18}F-FDG PET/CT aids in the detection of metastases and provide guidance for diagnosis and staging. Future studies with larger sample sizes are expected to refine imaging criteria and enhance diagnostic precision of ^{18}F-FDG PET/CT in CDC. These advancements will contribute to better patient management and prognosis for this rare renal neoplasm.

Acknowledgements

This work was supported by the Beijing Science Foundation for Distinguished Young Scholars (JQ21025), the National Natural Science Foundation of China (82171970), the Beijing Municipal Science & Technology Commission (Z221100007422027) and National High Level Hospital Clinical Research Funding (Interdisciplinary Research Project of Peking University First Hospital, 2023IR17).

Disclosure of conflict of interest

None.

Address correspondence to: Lei Kang and Tianyao Wang, Department of Nuclear Medicine, Peking University First Hospital, Beijing 100034, China. E-mail: kanglei@bjmu.edu.cn (LK); tianyao.wang@pkufh.com (TYW)

References

[1] Chao D, Zisman A, Pantuck AJ, Gitlitz BJ, Freedland SJ, Said JW, Figlin RA and Belldegrun AS. Collecting duct renal cell carcinoma: clinical study of a rare tumor. J Urol 2002; 167: 71-74.

[2] Karakiewicz PI, Trinh QD, Rioux-Leclercq N, de la Taille A, Novara G, Tostain J, Cindolo L, Ficarra V, Artibani W, Schips L, Zigeuner R, Mulders PF, Lechevallier E, Coulange C,

Valeri A, Descotes JL, Rambeaud JJ, Abbou CC, Lang H, Jacqmin D, Mejean A and Patard JJ. Collecting duct renal cell carcinoma: a matched analysis of 41 cases. Eur Urol 2007; 52: 1140-1145.

[3] Sui W, Matulay JT, Robins DJ, James MB, Onyeji IC, Roy-Choudhury A, Wenske S and DeCastro GJ. Collecting duct carcinoma of the kidney: disease characteristics and treatment outcomes from the National Cancer Database. Urol Oncol 2017; 35: 540.e513-540.e518.

[4] Tang C, Zhou Y, Ge S, Yi X, Lv H and Zhou W. Incidence, clinical characteristics, and survival of collecting duct carcinoma of the kidney: a population-based study. Front Oncol 2021; 11: 727222.

[5] Dimopoulos MA, Logothetis CJ, Markowitz A, Sella A, Amato R and Ro J. Collecting duct carcinoma of the kidney. Br J Urol 1993; 71: 388-391.

[6] Tannir NM, Plimack E, Ng C, Tamboli P, Bekele NB, Xiao L, Smith L, Lim Z, Pagliaro L, Araujo J, Aparicio A, Matin S, Wood CG and Jonasch E. A phase 2 trial of sunitinib in patients with advanced non-clear cell renal cell carcinoma. Eur Urol 2012; 62: 1013-1019.

[7] Sheng X, Cao D, Yuan J, Zhou F, Wei Q, Xie X, Cui C, Chi Z, Si L, Li S, Mao L, Lian B, Tang B, Yan X, Wang X, Kong Y, Dai J, Bai X, Zhou L and Guo J. Sorafenib in combination with gemcitabine plus cisplatin chemotherapy in metastatic renal collecting duct carcinoma: a prospective, multicentre, single-arm, phase 2 study. Eur J Cancer 2018; 100: 1-7.

[8] Gurel S, Narra V, Elsayes KM, Siegel CL, Chen ZE and Brown JJ. Subtypes of renal cell carcinoma: MRI and pathological features. Diagn Interv Radiol 2013; 19: 304-311.

[9] Leveridge MJ, Bostrom PJ, Koulouris G, Finelli A and Lawrentschuk N. Imaging renal cell carcinoma with ultrasonography, CT and MRI. Nat Rev Urol 2010; 7: 311-325.

[10] Elstob A, Gonsalves M and Patel U. Diagnostic modalities. Int J Surg 2016; 36: 504-512.

[11] Kay FU and Pedrosa I. Imaging of solid renal masses. Urol Clin North Am 2018; 45: 311-330.

[12] Hu Y, Lu GM, Li K, Zhang LJ and Zhu H. Collecting duct carcinoma of the kidney: imaging observations of a rare tumor. Oncol Lett 2014; 7: 519-524.

[13] Hwang SH, Cho A, Yun M, Choi YD, Rha SY and Kang WJ. Prognostic value of pretreatment metabolic tumor volume and total lesion glycolysis using 18F-FDG PET/CT in patients with metastatic renal cell carcinoma treated with anti-vascular endothelial growth factor-targeted agents. Clin Nucl Med 2017; 42: e235-e241.

[14] Tokuda N, Naito S, Matsuzaki O, Nagashima Y, Ozono S and Igarashi T; Japanese Society of Renal Cancer. Collecting duct (Bellini duct) renal cell carcinoma: a nationwide survey in Japan. J Urol 2006; 176: 40-43; discussion 43.

[15] Zhu Q, Wu J, Wang Z, Zhu W, Chen W and Wang S. The MSCT and MRI findings of collecting duct carcinoma. Clin Radiol 2013; 68: 1002-1007.

[16] Pickhardt PJ, Siegel CL and McLarney JK. Collecting duct carcinoma of the kidney: are imaging findings suggestive of the diagnosis? AJR Am J Roentgenol 2001; 176: 627-633.

[17] Zhu Q, Ling J, Ye J, Zhu W, Wu J and Chen W. CT and MRI findings of cystic renal cell carcinoma: comparison with cystic collecting duct carcinoma. Cancer Imaging 2021; 21: 52.

[18] Yoon SK, Nam KJ, Rha SH, Kim JK, Cho KS, Kim B, Kim KH and Kim KA. Collecting duct carcinoma of the kidney: CT and pathologic correlation. Eur J Radiol 2006; 57: 453-460.

[19] Lyu Z, Liu L, Li H, Wang H, Liu Q, Chen T, Xu M, Tian L and Fu P. Imaging analysis of 13 rare cases of renal collecting (Bellini) duct carcinoma in northern China: a case series and literature review. BMC Med Imaging 2021; 21: 42.

[20] Ge J, Zuo C, Guan Y and Liang Z. Enhanced MRI and 18F-FDG PET/CT findings of preoperative primary renal collecting duct carcinoma. Clin Nucl Med 2016; 41: 998-999.

[21] Ye XH, Chen LH, Wu HB, Feng J, Zhou WL, Yang RM, Bu ZB, Ding Y, Guan J and Wang QS. 18F-FDG PET/CT evaluation of lymphoma with renal involvement: comparison with renal carcinoma. South Med J 2010; 103: 642-649.

[22] Wang HY, Ding HJ, Chen JH, Chao CH, Lu YY, Lin WY and Kao CH. Meta-analysis of the diagnostic performance of [18F]FDG-PET and PET/CT in renal cell carcinoma. Cancer Imaging 2012; 12: 464-474.

[23] Zukotynski K, Lewis A, O'Regan K, Jacene H, Sakellis C, Krajewski K and Israel D. PET/CT and renal pathology: a blind spot for radiologists? Part 1, primary pathology. AJR Am J Roentgenol 2012; 199: W163-167.

[24] Zukotynski K, Lewis A, O'Regan K, Jacene H, Sakellis C, Almodovar S and Israel D. PET/CT and renal pathology: a blind spot for radiologists? Part 2--lymphoma, leukemia, and metastatic disease. AJR Am J Roentgenol 2012; 199: W168-174.

[25] Tsui KH, Shvarts O, Smith RB, Figlin RA, deKernion JB and Belldegrun A. Prognostic indicators for renal cell carcinoma: a multivariate analysis of 643 patients using the revised 1997 TNM staging criteria. J Urol 2000; 163: 1090-1095; quiz 1295.

[26] Safaei A, Figlin R, Hoh CK, Silverman DH, Seltzer M, Phelps ME and Czernin J. The usefulness of F-18 deoxyglucose whole-body positron emission tomography (PET) for restaging of renal cell cancer. Clin Nephrol 2002; 57: 56-62.

[27] Majhail NS, Urbain JL, Albani JM, Kanvinde MH, Rice TW, Novick AC, Mekhail TM, Olencki TE, Elson P and Bukowski RM. F-18 fluorodeoxyglucose positron emission tomography in the evaluation of distant metastases from renal cell carcinoma. J Clin Oncol 2003; 21: 3995-4000.

[28] Li D, Fu C, You Y, Zhang Q and Zhang X. A rare collecting duct carcinoma with widespread metastasis visualized by 18F-FDG PET/CT. Clin Nucl Med 2022; 47: 93-95.

[29] Marx K, Bauer J, Guillou L, Delaloye AB and Prior J. Bellini duct carcinoma: visualization on F-18 FDG PET/CT. Clin Nucl Med 2009; 34: 541-2.

[30] Bertagna F, Fisogni S, Tardanico R, Simeone C, Cunico SC and Giubbini R. 18F-FDG PET/CT in a patient affected by renal collecting duct (Bellini) carcinoma. Clin Nucl Med 2012; 37: 986-8.